Microplasma device with graphene cathode

H. HİLAL YÜCEL KURT*, S. UTAŞ*
Department of Physics, Faculty of Science, Gazi University, 06500 Teknikokullar, Ankara, Turkey

Graphene is used as a cathode material in a microplasma device. Graphene is suitable for plasma systems in terms of excellent conductivity, spatial charge density, and distribution of electrons moving between the anode and cathode. The progressive development of semiconductor technology is based on small chips containing a cathode-anode couple, along with the development of micro and nanoparticles. Graphene is used as a cathode material instead of semiconductor material for the first time to our knowledge. As a new and developing trend, the modeling of plasma systems, cell designs and ideal operating conditions are still being researched theoretically and practically. Plasma treatment of the materials has an important place in technology with increasing plasma studies in recent years. Plasma processing of fascinating materials such as graphene is critical in the aerospace, optical and paper industries, automotive, steel, and biomedical. Graphene has excellent conductivity, and caused high electron density in the plasma system according to our simulation results. Furthermore, an environmentally friendly microplasma device can be achieved with graphene cathode and thus can enhance the efficiency of the plasma system under stable and reliable conditions.

1. Introduction

Plasma technology has a strong application for nanotechnological studies and it has attracted great attention in recent years [1,3].Townsend discharge is one of the plasma ionization processes in which electrons are accelerated in a sufficiently strong electric field, causing the change in electrical conductivity due to the increasing avalanche mechanism. When a decrease in the number of free charges or in the electric field occurrs, this process stops the Townsend discharge. Townsend discharge got its name from John Sealy Townsend and is also known as the "Townsend avalanche mechanism". Avalanche means a successive reaction process in the plasma area for a sufficiently high electric field. This reaction takes place in an ionizable medium, such as air and argon. In this work, the calculations are made for both Townsend and glow discharge modes. Glow discharge has higher discharge light emissions and current densities.

Graphene is a very attractive material used in transistors, computer chips, power generation, small and efficient biosensor devices, and supercapacitors [1,2]. It has interesting light-absorbing abilities and absorbs 2.3% of white light. It is a competitor to its equivalents such as copper and silicon with its low active resistance structure at room temperature. So, it is used in this study as a cathode material in a microplasma device under Townsend discharge. Graphene is one of the rare examples of two-dimensional planar structures. It is a material made of pure carbon, similar to graphite but of two-dimensional structure with properties that make it extraordinarily light and strong. One square meter of graphene has a mass of 7 $\times$ 10^{-4}kg. Its strength is 200 times that of steel, and its density is similar to that of carbon fiber [4]. Graphene is one of the most conductive materials for electricity and heat, and is an excellent material for electronics and many other industries. Graphene is also chosen for its superior properties such as mobility, conductivity, and mechanical strength. Graphene, which is used as a cathode in this study, is also used in other detectors for (infrared, gamma, X-ray, etc.) radiations.

Graphene-based supercapacitors have exceptional energy storage properties. Because they have layered structures, large effective surface areas, and high electrical conductivity [5]. Further, many investigations have been made on graphen-plasma formations [6,7]. The applications have a wide range from pressure sensing [8], to gas sensing [9].

Graphene is used in our daily life such as phone, computer, tablet etc. Further, its usage areas cover solar cells [10], drug delivery, treatment of many diseases (targeting cancerous cells and reducing damage to healthy cells during chemotherapy) [11], plasma systems, foldable screens, touch panels, communications, photon transmission, industry, and modern power grids [12]. Graphene is the first known two-dimensional material [13] and with this feature, it attracts a lot of attention in terms of technological applications. Carbon nanotubes [14], which are the rolled form of graphene, are used in thousands of areas from electronics to health. It is also possible to tailor graphene in the areas envisioned for carbon nanotubes. Graphene is stronger than steel, more conductive than copper, more flexible than rubber, and more conductive than copper [15]. The most important property of graphene is that it is 100 to 300 times stronger than steel. Graphene is the thinnest and lightest material known [16].

In this study, an effort is made to find undetermined plasma parameters such as current density, space charge density, and migrating electron flux by incorporating gas

flow using the plasma module of COMSOL Multiphysics to make clear the sophisticated parameters for microplasma device with graphene cathode. Model results clarified the complex behavior of the plasma. By analyzing mean electron fluxes, space charge densities, and current densities, the contributions of the different plasma parameters for the device physics in the optimal operation range are explored.

2. Plasma cell formation and simulation graphics

Plasma is electrically neutral to the external environment. That is, the number of positive charges in the plasma is equal to the number of negative charges. All the opposite of these events, such as dissociation, ionization, and recombination, occur continuously in the plasma. These events are in constant motion on a graphene cathode. Fig. 1 shows the geometric structure of the plasma cell with a graphene cathode. Fig. 2 shows the mesh structure of the microplasma device.

In our system, graphene is defined as the cathode, while SnO_2-coated- glass is defined as the anode. In the first stage, the geometric structure was created. Then, argon gas and graphene have been chosen from the material library. COMSOL Multiphysics package gives the facility for the modeling of material-plasma systems. The numerical calculation is an important tool to improve our knowledge based on the plasma behavior inside the micro discharge cell with graphene electrodes, and it is also important to increase the knowledge in the field of dc micro discharges used for deposition or etching [17, 18]. The optimal mesh numbers used 42560 elements. The programme uses gas discharge formalism and the required material constants to find the steady-state solutions for the defined simulation cell [19]. It should be noted that according to our knowledge, there has been no published study on the graphene- plasma structure for microplasma system up to now.
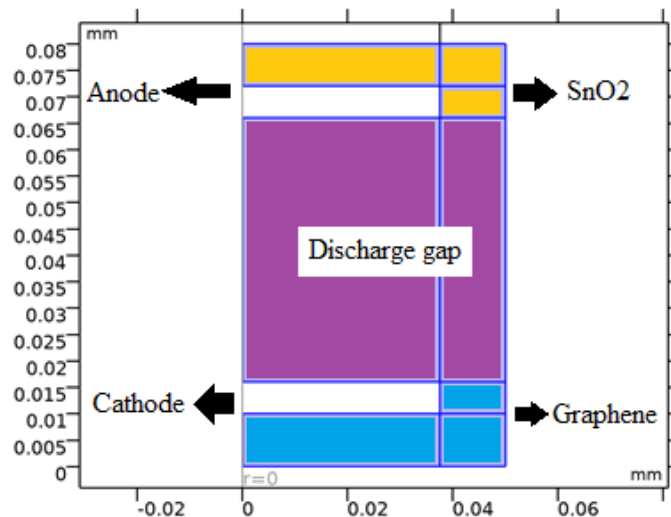

Fig. 1. Geometric structure of the plasma cell for d = 50 µm distance between anode and cathode (color online)
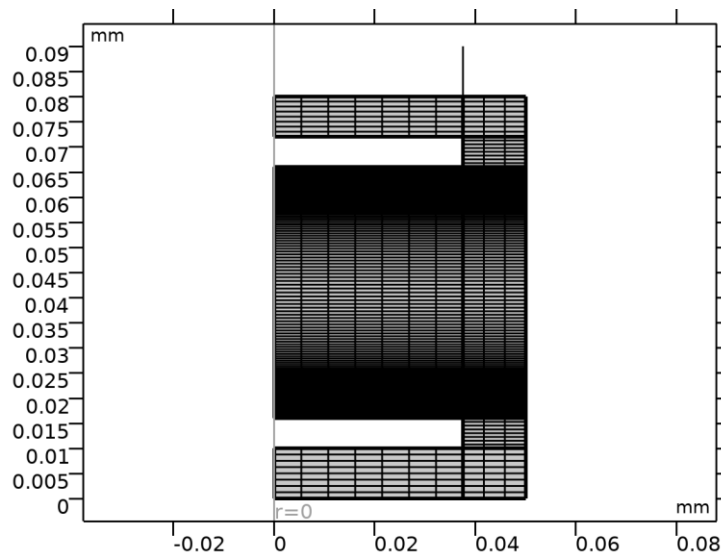

Fig. 2. The mesh of the investigated structure for graphene cathode

Because of many successive ionizations in the plasma range, the gas emits light in the visible range depending on the gas type and external conditions [6, 20]. When an electron gaining electrical energy has energy greater than its ionization potential, it causes gas atoms to vibrate, increasing their kinetic energy. Gas atoms with increased kinetic energy produce two slow electrons. The produced slow electrons are again increased in kinetic energy and accelerated by the effect of electric field. So, four electrons are produced by the effect of ionization. All these sequential formations are elements of the DC discharge that provides the formation of the plasma [21]. Many types of collisions are observed during this gas discharge phase. The most common are elastic collisions. This collision is the routine scattering of an electron from a neutral atom or a neutral-neutral collision. All other collisions are of the inelastic type. Elastic collisions consume a small fraction of electron energy due to the electron and molecular mass difference. In an inelastic collision, the gas excites the molecules or completely excites the electron and ionizes them. A DC gas discharge tube cell [17, 18, 22, 23] and the chemical reactions occurring in the cell [22] are shown in the figures below. Fig. 3 shows the basic cathode-anode tube. Fig. 4 shows the successive ionization processes in a plasma structure.
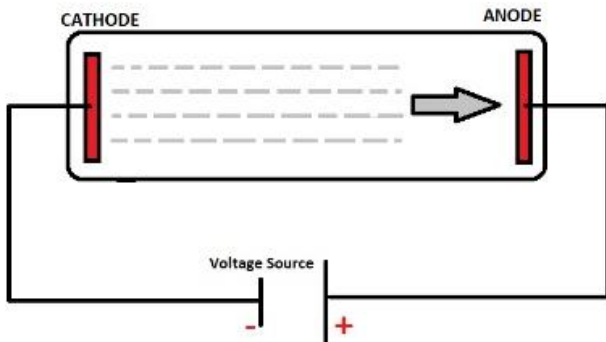

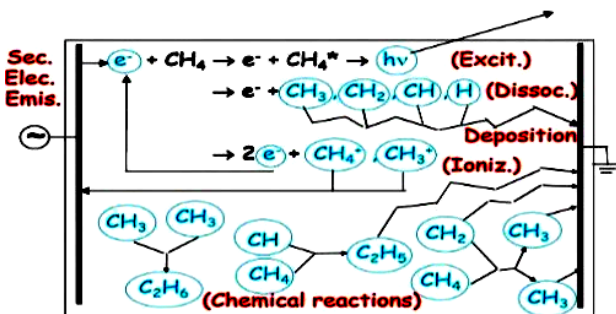*Fig. 3. Example of discharge tube [17, 18, 22, 23] (color online)*

Fig. 4. Example of the gas discharge reactions [22] (color online)

Plasma equations are given below. Many complex processes exist in a plasma structure.

With the drift-diffusion equation, the solutions of electron density and mean electron distribution can be produced [19, 24, 25, 26, 27].

$$\frac{\partial}{\partial t}(n_e) + \nabla.[-n_e (\mu_e . \vec{E} E - D_e \nabla n_e] = R_e \quad (1)$$

$$\frac{\partial}{\partial t}(n_\varepsilon) + \nabla.[- n_\varepsilon (\mu_\varepsilon . \vec{E} E) - D_\varepsilon \nabla n_\varepsilon] + \vec{E} E \Gamma_\varepsilon = R_\varepsilon \quad (2)$$

$$\Gamma_e = - (\mu_e . \vec{E} E) n_e - D_e . \nabla n_e \quad (3)$$

where R_e is the electron source rate and R_ε is the energy loss due to inelastic collisions; n_e is the electron density, μ_e is the electron mobility, $\vec{E}$ is the electrostatic field created by ambipolar diffusion, D_e is the the electron diffusivity, n_ε is electron density of energy loss resulting from inelastic collision, μ_ε is energy mobility, D_ε is the energy diffusivity, Γ_ε is the electron energy flux;

$$D_e = \mu_e T_e \quad (4)$$

$$\mu_\varepsilon = \left(\frac{5}{3}\right)\mu_e \quad (5)$$

$$D_\varepsilon = \mu_\varepsilon T_e \quad (6)$$

where T_e is the electron temperature.

Except for radio frequency (RF) discharges, secondary electron emission and discharge formation process are interrelated. When an ion hits the cathode, an electron is emitted with a certain probability from the cathode surface. When these electrons then get enough energy to initiate ionization, they are accelerated by a strong electric field near the cathode. Electrons can be lost due to their random movement at a few mean free path distances from the plasma wall and gain momentum due to the secondary emission mechanism, resulting in the following boundary condition. That is the electron flux condition [27]:

$$n.\Gamma_e = \left(\frac{1}{2}\right)v_{e,th} n_e) - \sum_p \gamma_p(\Gamma_p .n) \quad (7)$$

and the electron energy flux,

$$n.\Gamma_\epsilon = \left(\left(\frac{5}{6}\right)v_{e,th} n_\epsilon\right) - \sum_p [\epsilon_p \, \gamma_p \, (\Gamma_p.n)] \quad (8)$$

where n is the number of electrons reaching the anode; γ_p is secondary emission coefficient from the ion species; Γ_p is the positive ion flux and $v_{e,th}$ is the moving mass velocity.
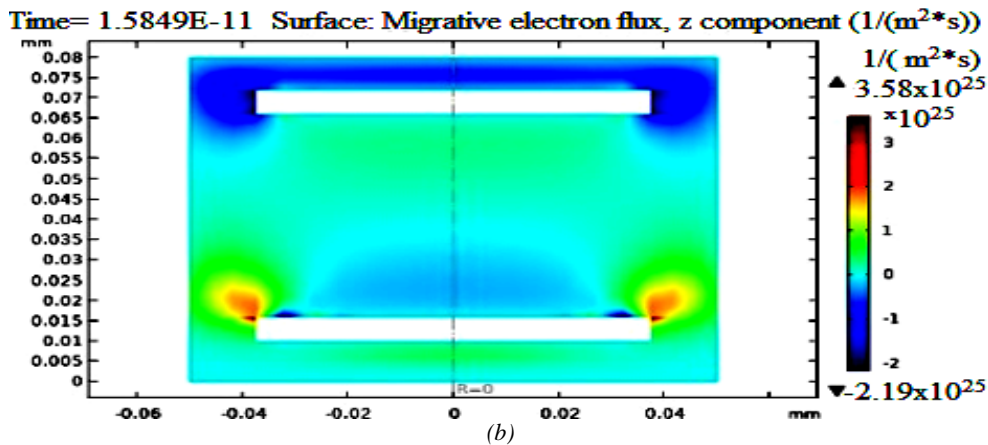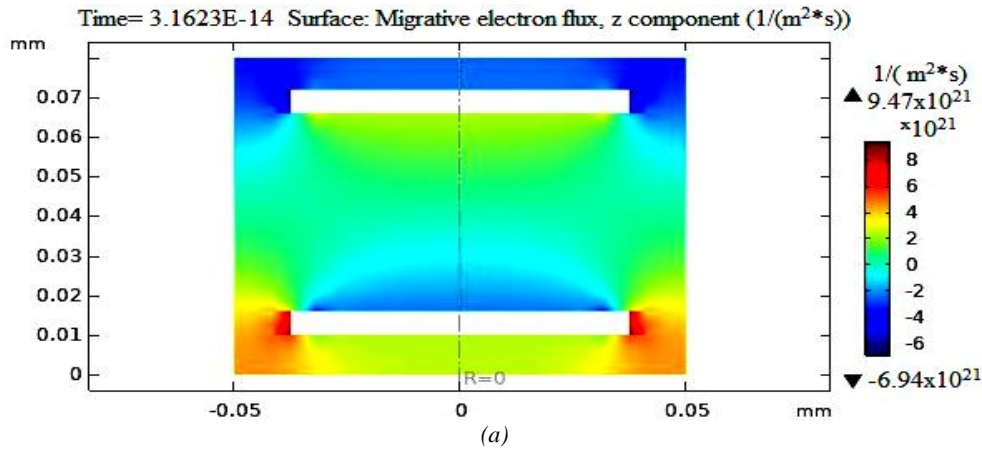
There are two types of electron populations; slow and fast. Fast electrons are electrons close to the cathode. The red-colored parts in the migrative electron flux plots represent the hot potential and the fast-moving parts, while the blue and yellow-colored parts in these plots represent the cold potential, or the slow-moving parts. Slow electrons are those that are released as a result of the ionization effect.

In this study, graphene material was chosen as the cathode in an argon gas environment. Because argon gas

has a strong diffusion feature at the point of interest and easily reacts with the III-V group and II-VI group semiconductor materials [28].

The electron mobility of the gas, collisions, experimental setup, DC power supply, resistors, capacitors, boundary equations, necessary formulas, and other necessary data were added to the Comsol Multiphysics program and the simulations were repeated by changing the distances between the anode and the cathode at different pressure values. In the results, electron density, spatial charge density, migrating electron, and electron current density formations were added to determine the suitability of graphene for the detector structure when it is used as a cathode material in the microplasma device. Fig. 5(a-e) identifies the high-energy electron regions within a large-density electron enhancement in plasma. The red color corresponds to hot and high-energy electrons. These high energetic electrons can start the cathode glow at a certain distance from the cathode that corresponds to the average free path in the micro distance. Fig. 5(a-e) also shows the dynamic evolution of the migrative flux change with pressures, where the distribution of the migrative electron fluxes is shown for d = 50 μm. The migrative electron flux is changing with the gas pressure. The minimum value is obtained for p = 10 Torr (9.47×10^{21} 1/(m^2.s))and the

maximum value is obtained for p = 15 Torr (3.58×10^{25}1/(m^2.s)) as shown in Fig.5a and Fig. 5b, respectively. The plasma has complex dynamics and chemical successive ionizations. Many parameters have influence on the results as well as those related to the cathode. The flux divergence is due to the electron potential gradient as well as the pressure change in plasma. From finite element analysis, it can be observed that the electron migrative flux depends on plasma structure, electric field strength, pressure, and discharge distance between the cathode and anode. The migrative electron flux is found to be 9.93×10^{24} 1/(m^2.s)) for p = 22 Torr (Fig.5c), 5.14×10^{24} 1/(m^2.s)) for p =44 Torr. (Fig. 5 d), and p =3.83×10^{24} 1/(m^2.s)) for 66 Torr (Fig.5e). The general form of the computed patterns shown in Fig. 5(a-e) is different from each other depending on the plasma formation process. The characteristics of the emitted gas discharge depend on many parameters including both cathode material and the working gas. It has been found that there is an axially symmetric electron distribution with increasing pressure. The glow at the axial size of the cathode depends on the pressure of the gas and the type of gas discharge. Self-organized electron flux patterns have complex plasma chemistry due to nonlocal electric field strength in a glow discharge mode.
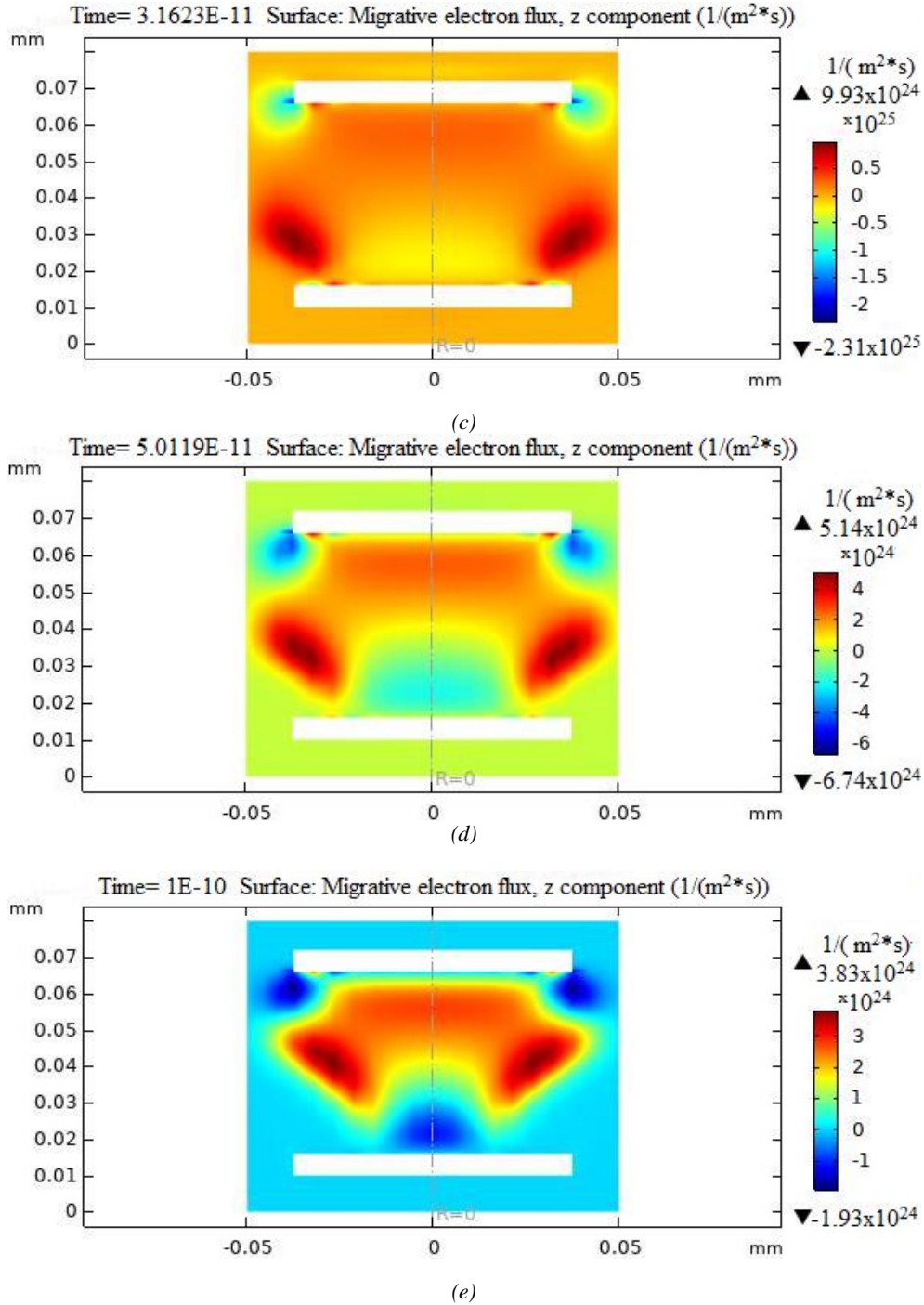

(a)

(b)

Time= 3.1623E-11 Surface: Migrative electron flux, z component (1/(m²*s))

(c)

Time= 5.0119E-11 Surface: Migrative electron flux, z component (1/(m²*s))

(d)

Time= 1E-10 Surface: Migrative electron flux, z component (1/(m²*s))

(e)

Fig. 5(a-e)Migrative electron flux for(a) p=10 Torr.(b) p=15 Torr.(c) p=22 Torr. (d)p=44 Torr.(e).p=66 Torr under 2000 V applied voltage (color online)

Surface electron current densities are shown in Fig. 6(a-b).The calculation is performed for p=100 Torr and 760 Torr at d =50 μm. Results demonstrate that the value of the surface electron current density is higher for p = 100 Torr with a value of 1.25×10^5 A/m², while its value for p=760 Torr is 1.16×10^5 A/m². Surface electron current density is distributed around the cathode as two symmetrical parts for p=100 Torr. It is observed that electrons have different energies in the plasma. Therefore, electrons with the same average energy distributions have clustered in the same area. The simulation is performed at low and high pressures to understand the self-organized plasma patterns based on the same applied voltages and interelectrode distance *d*.
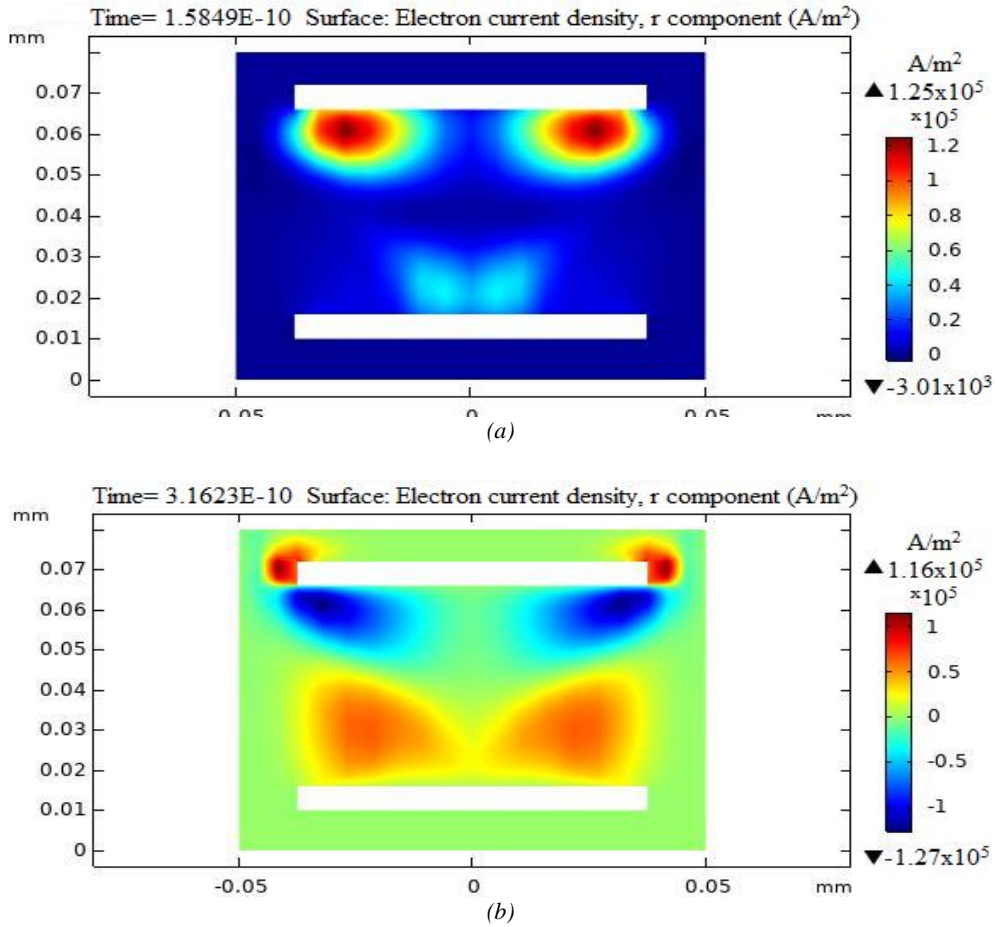
Fig. 6. (a-b) Surface electron current density patterns for a) p = 100 Torr, and b) p = 760 Torr (color online)

After the bombardment of the cathode surface with positive ions, the cathode emits electrons. This mechanism is called secondary electron diffusion. Aston dark region next to the semiconductor cathode can be seen in the microplasma device. This region has a strong electric field and a negative space charge. Therefore, Aston dark space or primary dark space is formed in front of the cathode by the accumulation of the secondary electrons.

Fig. 7(a-b) shows space charge densities for p = 300 Torr and p = 760 Torr. Space charges are positive charges and they are responsible for secondary electron emissions from the cathode. Energy exchange in plasma occurs between electrons and ions. They can make successive elastic and inelastic collisions even by giving their energies to the boundary. The space charge is around 3.39 C/m^3 for p = 300 Torr, and 4.2 C/m^3 for p = 760 Torr.
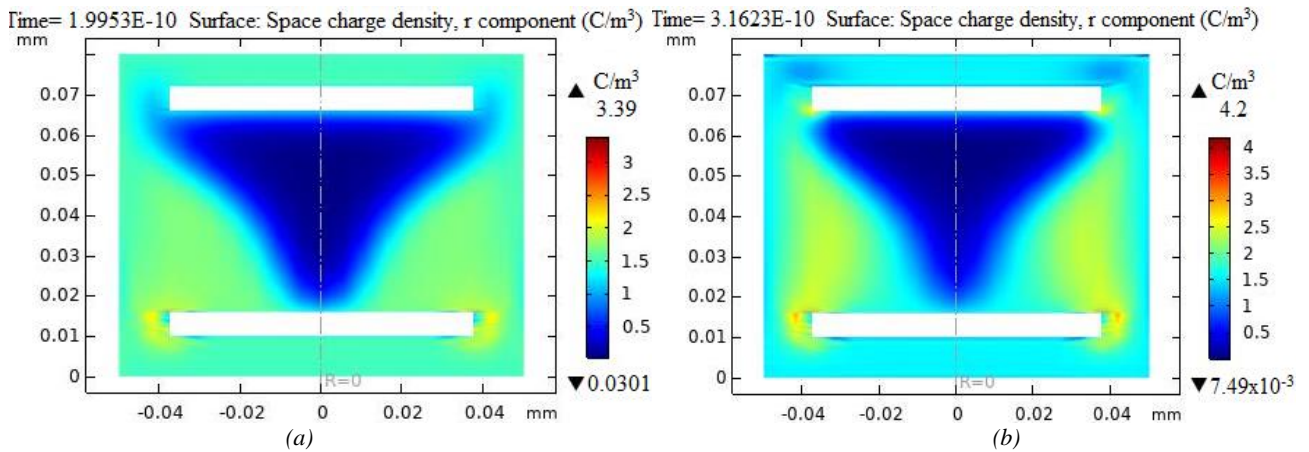

Fig. 7. (a-b) Space charge densities: a) for 300 Torr, and b) for 760 Torr at 2000 V (color online)

The atoms or molecules are ionized in an applied electric field, with the positive ions moving toward the cathode, and the free electrons moving toward the anode. If the electric field is strong enough, the electrons gain enough energy to release more free charge. With the collision of electrons with another atom or molecule, more electrons are released when it reaches a sufficient energy level.

The energy gained by the electrons along the mean free path is characterized by E/p. Electron avalanches evolve not only in time, but also in space, along the direction of the electric field. During these complex solutions in E/p, the breakdown curves obtained according to Paschen's law are determined by a certain inter-electrode distance and pressure. E/p expresses the optimal value of the magnitudes corresponding to the minimum point of the Pashen curve. In other words, it is a critical parameter that indicates optimum plasma performance.

The strong bombardment of the surfaces of the electrodes by the electron-ion beam is characteristic on breakdown region and it begins at lower E/p values, where most of the energy is lost by the electrons in ionization due to severe Penning ionization [24].

In experimental and theoretical measurements, the results must be accurate and realistic. Because the wrong analysis may be made while researching the problem, not enough information about the problem may be available, or the experiment set or equations used in the problem may be missing, and the solution may be incorrect. To eliminate these problems, uncertainty analysis needs to be performed. A reference value must be compared with the results to establish a margin of error.

3. Uncertainty analysis

Uncertainty analysis gives us more information about the accuracy of the results and their closeness to realistic measurements. Measurements are carried out small intervals and the margin of error between the reference value will eliminate the uncertainty [29]. Since the system is completely simulation-oriented, the plasma and electrical circuit modules and their equations embedded in the simulation program have reduced uncertainty. But the reference value is of great importance. In this section, the

error margins for the migrating electron flow of different pressures are shown by keeping the voltage of 2000 Volts constant in an argon plasma under 760 Torr pressure. The migrating electron flow in 2000 Volt argon plasma under 760 Torr pressure was found to be 1.96×10^{24} $1/(m^2.s)$. The simulation solution range varies in small time intervals. In this way, a more precise and realistic value is expected to be created. The closer the margin of error is to 1, the more accurate andrealistic it is.
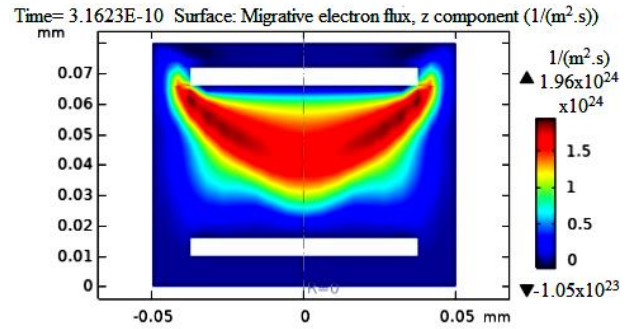

Fig. 8. Migrative electron flux forp=760 Torr pressure and U = 2000 V voltage at a solution time interval (-13.5 s)-(-9.5 s) (color online)

When the simulation calculations were obtained for pressure value of 22 Torr and applied voltage of 2000V, the result increased from 1.96×10^{24} to $4.39 \times 10^{24} 1/(m^2.s)$ for Fig. 9 (a).The value of WU indicates the margin of error in uncertainty analysis. The absolute value of the results was taken. Here, the flux is symbolized as $k1$ for 22 Torr pressure, and the flux is symbolized as k for 760 Torr pressure. The margin of error for these two pressures is;

$$WU = [(k1-k)/k] = 1.23 \qquad (9)$$

Likewise, the result changed from 1.96×10^{24} to $1.26 \times 10^{24} 1/(m^2.s)$ as shown below;

$$W_U = [(k_1-k)/k] = [0.7 \times 10^{24}/1.96 \times 10^{24}] = 0.35 \qquad (10)$$

(a)

(b)

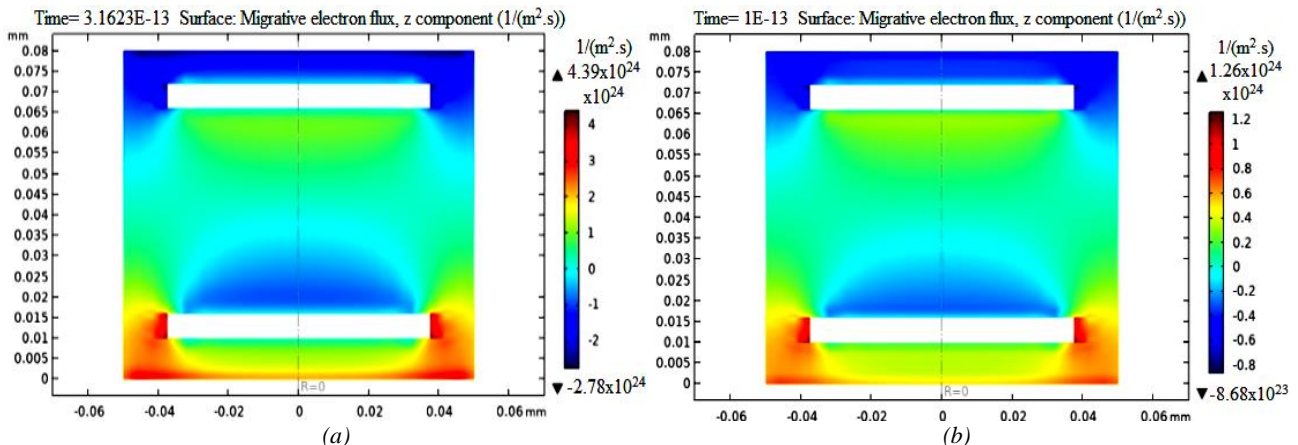*Fig. 9. (a-b)Migrative electron flux for p=22 Torr pressure and U = 2000 V voltage at a solution time interval: (a) for (-13.5 s)-(-13 s)b) for (-13.5 s)-(-12 s)*

When the plasma pressure was decreased from 760 Torr to 44 Torr and the solution range is kept short under 2000V, the electron flow rate between cathode and anode decreased from 1.96×10^{24} to 6.37×10^{23} $1/(m^2.s)$, and the result of uncertainty is as follows;

$$W_U = [(k_2-k)/k] = 0.675 \qquad (11)$$

$k2$ is the migrating electron flux value under 44 Torr pressure for Fig. 10(a). Likewise, when looking at a second solution range for $p = 44$ Torr, the electron flow rate decreased from 1.96×10^{24} to 3.03×10^{23} $1/(m^2.s)$, and its value is 0.845:
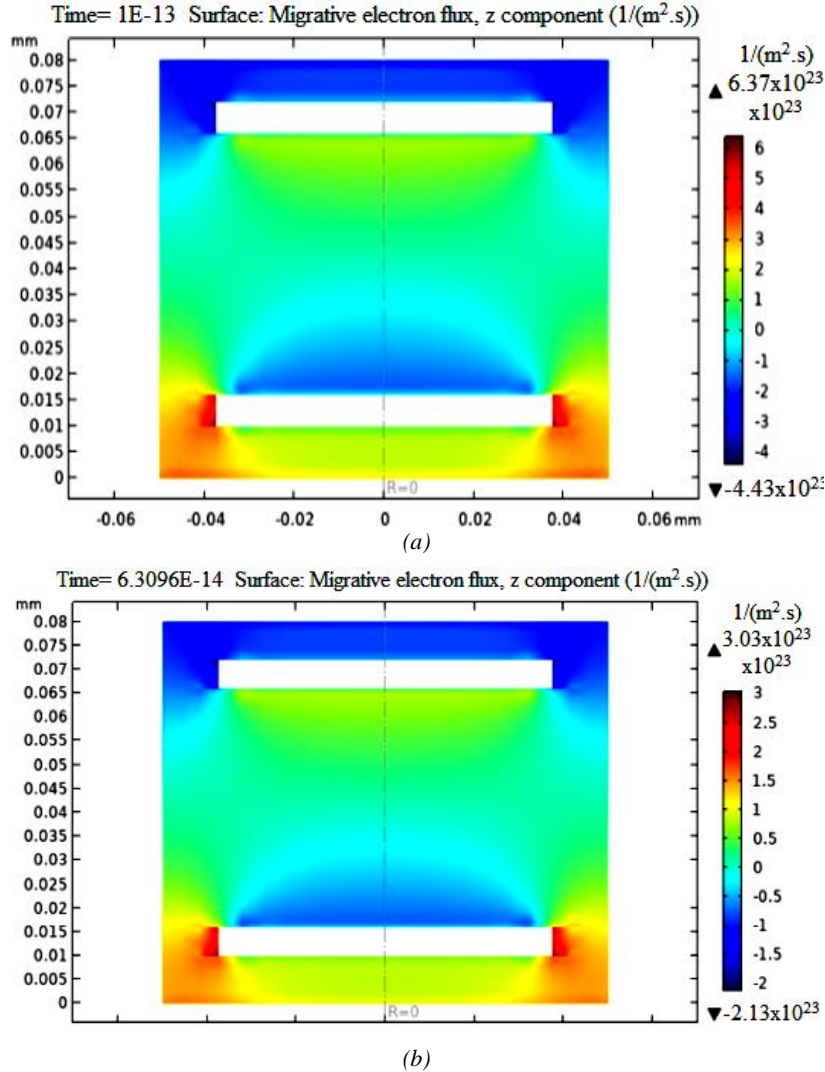
$$W_U = [(k_2-k)/k] = 0.845 \qquad (12)$$

(a)

(b)

Fig.10. (a-b)Migrative electron flux for p=44Torr pressure and U = 2000 V voltage at a solution time interval: a) for(-13.5 s)-(-13 s)b)for(-13.5 s)-(-12 s) (color online

When the solution time of the plasma cell is calculated with short interval under $p = 66$ Torr and applied voltage = 2000 V, the electron flow rate decreased from 1.96×10^{24} to 1.2×10^{23} $1/(m^2.s)$ and 5.45×10^{22} $1/(m^2.s)$ for Fig. 11 (a) and (b), respectively.

Uncertainy analysis is 0.938 for Fig. 11 (a) as follow;

$$W_U = [(k_3-k)/k] = 0.938 \qquad (13)$$

$k3$ is the migrating electron flux value for 66 Torr pressure. Uncertainy analysis is 0.972 for Fig. 11 (b) as stated below:

$$W_U = [(k_3-k)/k] = 0.972 \qquad (14)$$

When the results are examined, it can be seen that the margin of error decreases and approaches 1 with increase in the pressure.
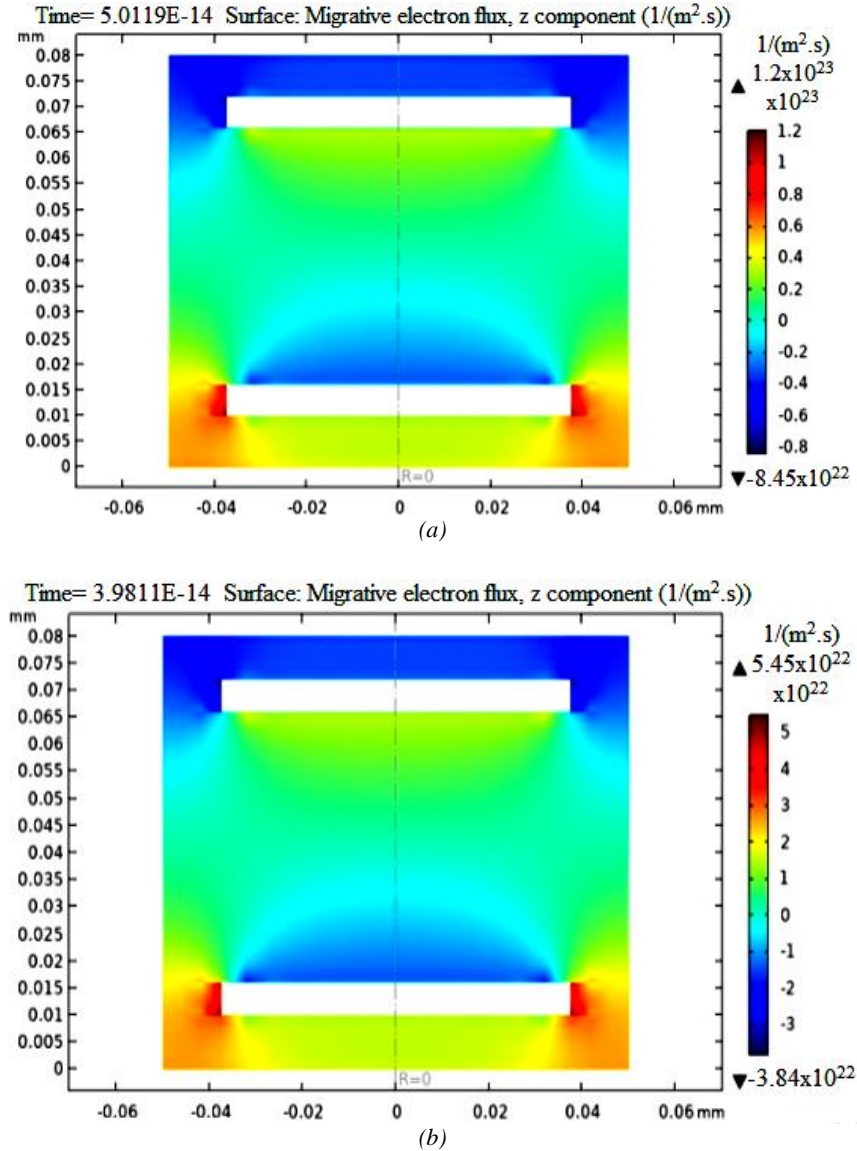
Time= 5.0119E-14 Surface: Migrative electron flux, z component (1/(m².s))

(a)

Time= 3.9811E-14 Surface: Migrative electron flux, z component (1/(m².s))

(b)

Fig. 11. (a-b)Migrative electron flux values for 66 Torr and U = 2000 V voltage at a solution time interval:a) for (-13.5 s)-(-13 s) (b)for(-13.5 s)-(-12 s) (color online)

4. Conclusion

The COMSOL simulation program was used to obtain electron current densities, space charge accumulation, and migrative electron flux for graphene cathode in the microplasma device. It is found that both electron current density and space charge are associated with the pressure changes in the plasma and collisions with argon gas, as well as their positions change with pressure.

3D MEE maps have been calculated using the COMSOL simulation programme which uses a two-term Boltzmann equation [30] to calculate the electron energy distributions for regular plasma patterns which are formed in plasma boundaries. In this work, an effort has been made to find undefined plasma parameters such as migrative electron fluxes and electron current densities by incorporating the gas flow using the plasma module of COMSOL Multiphysics. Model results clarified the complex behavior of the plasma to increase the knowledge

about studies of plasma-related cells for the optimization of future device applications. In current calculations, the minimum migrative flux is found to be $(9.47 \times 10^{21}$ $1/(m^2.s))$ for p = 10 Torr and the maximum value is found to be $(3.58 \times 10^{25}$ $1/(m^2.s))$ for p = 15 Torr. The aspect of the migrative flux is changing with pressure and values are between $(9.47 \times 10^{21}$ $1/(m^2.s))$ and $(3.58 \times 10^{25}$ $1/(m^2.s))$.

Furthermore, it is found that electron current densities for graphene cathode are 1.25×10^5 A/m^2 for p = 100 Torr, and 1.16×10^5 A/m^2 for p = 760 Torr. However, space charge densities have the higher value of (4.2 C/m^3) for p = 760 Torr compared to (3.39 C/m^3) for p = 300 Torr.

It is observed that graphene cathode caused higher ionization in plasma when compared to our studies that were made previously for semiconductor cathodes. Plasma science has advantage in the field of nanotechnology. This study will make progress for future studies based on Graphene cathode for microplasma device applications. However, extensive studies have to carry out for

optimization of the microplasma systems with graphene cathode. Difficulties in achieving stability put limitations on the plasma system. Unstable plasma causes nonlinear current density and nonuniform electric field [31-33]. If we provide the uniform plasma, the plasma systems can be used for the development of a large area microplasma-based ultraviolet light source with graphene cathode.

References

[1] U. Kamran, Y. J. Heo, J. W. Lee, S. J. Park, Micromachines **10**(4), 234 (2019).

[2] S. Eigler, Carbon **47**(12), 2936 (2009).

[3] Y. Q. Fang, W. Chen, T. H. Ao, C. Liu, L. Wang, X. J. Gao, H. Zhang, J. W. Pan, Review of Scientific Instruments **91**(8), 083102 (2020).

[4] Ezzatollah Shamsaei, Felipe Basquiroto de Souza, Yupei Yao, Emad Benhelal, Abozar Akbari, Wenhui Duan, Construction and Building Materials **183**, 642 (2018)

[5] N. Namdar, F. Ghasemi, Z. Sanaee, Scientific Reports **12**(1), 1 (2022).

[6] Y. T. Aladadi, M. A. Alkanhal, IEEE Transactions on Plasma Science **48**(4), 852 (2020).

[7] P. Fortugno, S. Musikhin, X. Shi, H. Wang, H. Wiggers, C. Schulz, Carbon **186**, 560 (2022).

[8] M. Šiškins, M. Lee, D. Wehenkel, R. van Rijn, T. W. de Jong, J. R. Renshof, P. G. Steeneken, Microsystems and Nanoengineering **6**(1), 1 (2020).

[9] J. H. Choi, J. Lee, M. Byeon, T. E. Hong, H. Park, C. Y. Lee, ACS Applied Nano Materials **3**(3), 2257 (2020).

[10] Z. Yin, J. Zhun, Q. He, X. Cao, C. Tan, H. Chen, Q. Yan, H. Zhang, Adv. Energy Materials **4**, 1300574 (2014).

[11] A. Yılmaz, Reduction of Surface Currents in Microwave Antennas Used in Cancer Treatment with Graphene-Like Material, 2016.

[12] Z. Zhen, H. Zhu, Structure and properties of graphenem Academic Press, 1 (2018).

[13] S. Z. Butler, S. M. Hollen, L. Cao, Y. Cui, J. A. Gupta, H. R. Gutiérrez, J. E. Goldberger,

ACS Nano **7**(4), 2898 (2013).

[14] I. A. Kinloch, J. Suhr, J. Lou, R. J. Young, P. M. Ajayan, Science **362**(6414), 547 (2018).

[15] T. M. Radadiya, European Journal of Material Sciences **2**(1), 6 (2015).

[16] A. K. Geim, K. S. Novoselov, Nature Materials **6**(3), 183 (2007).

[17] H. Y. Kurt, A. Inalöz, B. G. Salamov, Optoelectron. Adv. Mat. **4**(2), 205 (2010).

[18] H. H. Kurt, E. Tanrıverdi, Journal of Electronic Materials **46**(7), 3965 (2017).

[19] D. Bimberg, N. Kirstaedter, N. N. Ledentsov, Z. I. Alferov, P. S. Kopev, V. M. Ustinov, IEEE Journal of Selected Topics in Quantum Electronics **3**(2), 196 (1997).

[20] N. Lu, Z. Li, Z. Yang, Journal of Physical Chemistry C **113**(38), 16741 (2009).

[21] I. Rafatov, E. A. Bogdanov, A. A. Kudryavtsev, Physics of Plasmas **19**(3), 033502 (2012).

[22] Neha Thakur, S. N. Vasudevan, Agricultural Reviews **42**(2), 197 (2021).

[23] H. H. Kurt, E. Tanrıverdi, Journal of Electronic Materials **46**(7), 4024 (2017).

[24] Ansgar Jüngel, Transport Equations for Semiconductors, Springer, Berlin, Heidelberg, 1 (2009).

[25] S. S. Kasymov, G. Paritskii, Russian Authors' Certificate **18**(10), 1798020 (1973).

[26] Y. SakiyamaD. B. Graves, H. W. Chang, T. Shimizu, G. E. Morfill, J. Phys. D: Appl. Phys. **45**, 425201 (2012).

[27] I. Rafatov, E. A. Bogdanov, A. A. Kudryavtsev, Phys. Plasmas **19**(3), 033502 (2012).

[28] S. J. Ikhmayies, H. H. Kurt (Eds.), Advances in Optoelectronic Materials, International Publishing, New York, Springer, 145 (2021).

[29] I. J. Good, Journal of statistical computation and simulation **52**(2), 192 (1995).

[30] S. Kawaguchi, K. Takahashi, H. Ohkama, K. Satoh, Science and Technology **29**(2), 025021 (2020).

[31] H. Kurt, S. Çetin, B. G. Salamov, IEEE Transactions on Plasma Science **39**, 1086 (2011).

[32] E. Kurt, B. Ciylan, O. O. Taskan, H. H. Kurt, Scientia Iranica **21**, 935 (2014).

[33] E. Ongun, H. H. Yücel Kurt, S. Utaş, J Mater Sci: Mater Electron **35**, 655 (2024).

───────────────────────────
*Corresponding authors: hkurt@gazi.edu.tr;
                  selcuk.utas@gmail.com